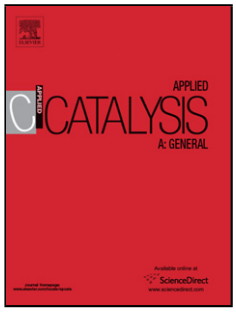

Title: Platinum, Palladium and Nickel supported on Fe_3O_4 as catalysts for glycerol aqueous-phase hydrogenolysis and reforming

Authors: André Von Held Soares, Hanan Atia, Udo Armbruster, Fabio Barboza Passos, Andreas Martin

PII: S0926-860X(17)30331-9
DOI: http://dx.doi.org/doi:10.1016/j.apcata.2017.07.023
Reference: APCATA 16328

To appear in: *Applied Catalysis A: General*

Received date: 8-4-2017
Revised date: 10-7-2017
Accepted date: 14-7-2017

Please cite this article as: André Von Held Soares, Hanan Atia, Udo Armbruster, Fabio Barboza Passos, Andreas Martin, Platinum, Palladium and Nickel supported on Fe3O4 as catalysts for glycerol aqueous-phase hydrogenolysis and reforming, Applied Catalysis A, Generalhttp://dx.doi.org/10.1016/j.apcata.2017.07.023

Platinum, Palladium and Nickel supported on Fe_3O_4 as catalysts for glycerol aqueous-phase hydrogenolysis and reforming

André Von Held Soares[a,b], Hanan Atia[c], Udo Armbruster[c], Fabio Barboza Passos*[a], Andreas Martin[c]

[a]*Departamento de Engenharia Química e de Petróleo, Universidade Federal Fluminense, Rua Passo da Pátria, 156, Niterói, RJ, CEP 24210-240, Brazil*

[b]*Instituto Federal do Rio de Janeiro – IFRJ, Avenida República do Paraguai, 120, Sarapuí– Duque de Caxias, RJ, CEP: 25050-100, Brazil*

[c]*Leibniz-Institut für Katalyse e.V. an der Universität Rostock, Albert-Einstein-Str. 29a, D-18059 Rostock, Germany*

*Corresponding author. E-mail address: fbpassos@vm.uff.br

Graphical abstract

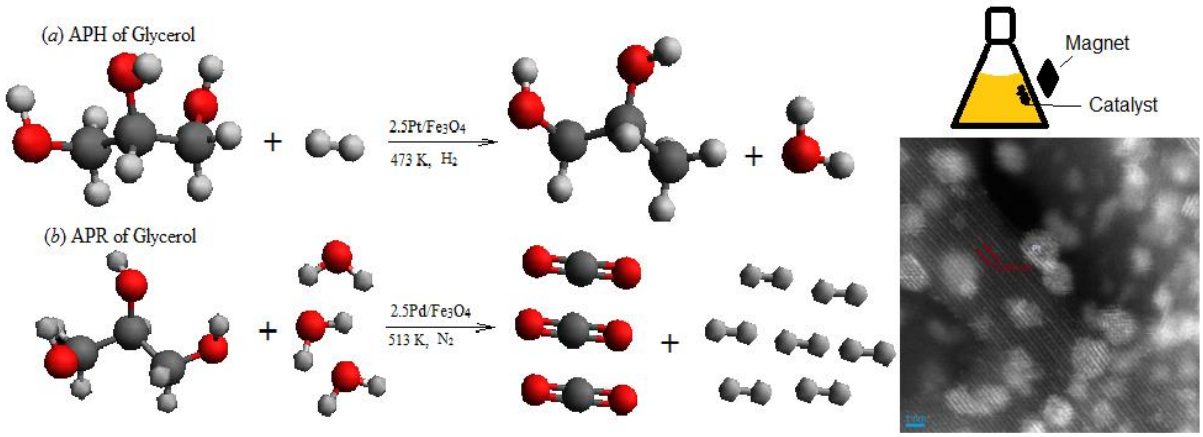

Highlights for "Platinum, Palladium and Nickel supported on Fe3O4 as catalysts for glycerol aqueous-phase hydrogenolysis and reforming" by Soares et al.

- Glycerol hydrogenolysis and reforming were studied on Pt, Pd and Ni/Fe_3O_4.
- Both for glycerol hydrogenolysis and APR, the activity order was Pt > Pd > Ni.
- Glycerol hydrogenolysis and reforming shared some of the reaction steps.
- 2.5Pt/Fe_3O_4 was active and stable.

ABSTRACT

Aqueous-phase hydrogenolysis (APH) and reforming (APR) are intertwined reactions with great interest for biomass valorization, as APR generates hydrogen *in situ* at preferred APH

reaction conditions instead of using external sources. We investigated iron oxide-supported Pt, Pd and Ni as catalysts for these reactions using glycerol as starting material. Catalysts were characterized by ICP, N_2 physisorption, H_2 chemisorption, XRD, TPR, CO_2-TPD, FTIR of pyridine adsorption, XPS and TEM. The catalyst tests were performed in an autoclave extended with an *in situ* pre-reduction setup. Hydrogen spillover was found from hydrogen chemisorption of Pt catalysts, and after the development of a custom-made methodology, the Pt particle size was found to be 1.8 nm for the 2.5Pt/Fe_3O_4 catalyst, which agrees with TEM analysis (1.56 nm). Both for hydrogenolysis and APR, the activity order was Pt > Pd > Ni, directly related to the stability of reduced small nanoparticles, which has an impact on acid-base properties of the support. Pt showed the best performance in hydrogenolysis even at a low content (81% conversion, 79% 1,2-propanediol selectivity for 1.0Pt/Fe_3O_4). The 2.5Pd/Fe_3O_4 catalyst showed the highest hydrogen yield in APR (69.2% at 513 K and 78.9% conversion). First order kinetic fits were made for 2.5Pt/Fe_3O_4, from which an apparent activation energy of 61.1 kJ·mol^{-1} was obtained and an initial turnover frequency (TOF_0) of 0.121 s^{-1}.

Keywords: Glycerol hydrogenolysis, APR, platinum, palladium, iron oxide, in situ pre-reduction

1. *Introduction*

Within the conceptual framework of biomass valorization, the transformation of glycerol into specialty and commodity chemicals cannot be overstated. Aqueous-phase hydrogenolysis (APH) and reforming (APR) of glycerol are intertwined reactions that differ from one another regarding the origin of hydrogen. While H_2 is externally fed and consumed in APH, H_2 is produced *in situ* from glycerol conversion in APR. The connection between these two reactions lies in the fact that they can be operated at the same hydrothermal conditions (200-250 °C, 20-50 bar), and by coupling both reactions, APR may serve as hydrogen source for APH, finally forming hydrocarbons, alcohols, polyols and carbonylated structures.

Hydrogenolysis is defined as the process of cleaving a C-X bond between a carbon and a hetero-atom or another carbon atom, followed by the addition of hydrogen to the cleaved fragments [1]. The probability of C-C bond cleavage also leads to formation of smaller molecules. The mechanism for hydrogenolysis of polyols may involve, however, stable intermediates, for which dehydration steps play an important role, such as, for example, acetol and acrolein in the case of glycerol conversion. The main liquid phase products of glycerol APH are 1,2-propanediol (1,2-PD), 1,3-propanediol (1,3-PD), 1-propanol (1-PrOH), iso-propanol (2-PrOH), hydroxyacetone (acetol), ethylene glycol (EG), ethanol and methanol. On the other hand, APR was developed as a process that generates hydrogen as a value-added product from aqueous carbohydrate solutions, especially from waste-water effluents [2]. Given that glycerol stems almost exclusively from biodiesel and soap production as a cheap by-product, its valorization may happen through both reactions using different catalysts [3,4].

Iron(III) oxide (Fe_2O_3) has many uses in catalysis, such as gas sensors [5], water splitting [6], water treatment [7], photocatalysis [8], dehydrogenation [9,10] and Fischer-Tropsch synthesis [11], to name a few. Fe_2O_3 is active for glycerol dehydration and hydrogen transfer, producing allylic alcohol, acetol and acrolein as the main products [12].

Catalysts that have platinum as the active metal and iron oxide as the support have been described in literature for many purposes, including electrocatalytic oxidation of ethanol [13], n-heptane isomerization [14] and the oxidation of formaldehyde [15]. In accordance to other studies on Pt-Fe catalysts applied to the reactions of the present work [16-18] we previously showed [19] that low contents of Fe enhance the activity of alumina-supported Pt catalysts via bimetallic particle formation.

The present work is a comparative study on the activity of platinum, palladium and nickel as active metals supported on iron oxide as catalysts in APH and APR of glycerol. Particular attention is given herein to Pt/Fe_3O_4. Although all metals belong to group 10 of the

periodic system, the catalytic activity varies greatly and pertinent characterization of materials is provided in order to clarify the connection between the catalyst's structure and its activity.

2. *Experimental*

2.1. *Catalyst preparation*

Active metals (Pt, Pd, and Ni) were added through incipient wetness impregnation using $H_2PtCl_6 \cdot 6H_2O$ (Alfa Aesar®), $PdCl_2$ (Alfa Aesar®), and $NiCl_2$ (Alfa Aesar®). For iron oxide preparation, 227.59 g of $Fe(NO_3)_3 \cdot 9H_2O$ were dissolved in 241 mL of H_2O, and 0.807 mL of an aqueous solution of 50 wt% of $Al(HPO_3)_3$ (Alfa Aesar®) were added. After mixing, water was distilled away under vacuum until a brown gel-like material was obtained. The gel was then calcined under 150 mL/min of air flow at 653 K for 1.5 hour, which was reached through heating at a rate of 2 K/min. After impregnation of the desired metals onto Fe_2O_3, the catalysts were once again calcined at 673 K for 4 hours with 4 K/min. All catalyst reductions at 523 K or lower were made using the autoclave setup described below. Reduction of the catalysts above 523 K was performed in a separate tubular quartz reactor. Fe_2O_3 nanocat (Sigma Aldrich®) was used as a reference material for BET surface area.

Throughout the present text, fresh calcined catalysts are labelled as X.XM/Fe_2O_3, where X.X is the metal content in wt%, and M the impregnated metal (Pt, Pd or Ni). Reduced catalysts are addressed as X.XM/Fe_3O_4 and were prepared using the autoclave *in situ* methodology, except for Fe_3O_4 and 2.5Ni/Fe_3O_4, which were reduced *ex situ* under hydrogen flow at 673 K.

2.2. *Catalyst characterization*

Chemical analysis was done by inductively coupled plasma-optical emission spectroscopy, using ICP-OES spectrometer Optima 3000XL (Perkin Elmer). Samples were

digested in a microwave oven (Anton Paar Multiwave from Perkin Elmer) with a mixture of aqua regia and HCl.

Surface area, pore volume and pore size distribution were determined by N_2 physisorption at 77 K, using an ASAP 2010 instrument from Micromeritics. Prior to the measurement, the samples were evacuated at 473 K and 0.1 mbar for 4 h. Surface area was calculated by BET method. Pore size distributions were calculated by the BJH method applied to the desorption step of the isotherm.

Hydrogen chemisorption was measured with an Autochem II 2920 equipment from Micromeritics. A tailor-made methodology was conceived and performed in order to assess and correct the spillover effect on $1.0Pt/Fe_3O_4$ and $2.5Pt/Fe_3O_4$. The methodology and its hypotheses are described in detail in the Supplementary Informarion document.

Temperature Programmed Reduction (TPR) was conducted with Autochem AC2920 from Micromeritics. After drying the catalyst under Ar flow, the reduction was performed with 50 mL/min of $5\%H_2/Ar$ at a rate of 10 K/min. The consumption of H_2 was monitored with a thermal conductivity detector.

X-ray powder diffraction (XRD) patterns were obtained using a STADI P automated transmission diffractometer (STOE, Darmstadt) with $CuK\alpha^1$ radiation and Ge monochromator. Scans were performed for 2θ within the range of 15-80° (step width 0.5°, 100 s/step) and recorded with a STOE position sensitive detector.

X-ray photoelectron spectra (XPS) were obtained with an ESCALAB 220iXL (ThermoScientific) with monochromatic AlKα radiation. The peak for C1s at 284.8 eV was used for calibration, and the spectra were fitted with Gaussian-Lorentzian curves for determination of the peaks' maxima and areas. All elements were analyzed from their principal peak.

Transmission electron microscopy (TEM) was performed using a Philips CM200 microscope equipped with a LaB6 filament and a supertwin lens operating at 200 kV. Bright-field images were acquired using a CCD camera (TVIPS GmbH). Samples of the catalyst powder were dispersed in ethanol with ultrasound, and drops of the dispersion were deposited on copper grids coated with amorphous carbon films. Particle were counted using ImageJ® software after setting the scale, selecting an evenly illuminated region of the micrograph, applying a bandpass filter and adjusting the threshold.

Basic sites of the catalysts were determined by temperature-programmed carbon dioxide desorption (CO_2-TPD) using an Autochem II 2910 equipment from Micromeritics. The samples were pretreated under 50 mL/min of He, and heated to 523 K at a rate of 10 K/min. Then they were cooled to 373 K and exposed to 50 mL/min of 1.2%CO_2/He for 90 min. After this, the samples were flushed with He still at 373 K for 30 min and then cooled to 343 K, the starting temperature of the analysis. Heating to 973 K was done at a rate of 10 K/min.

For acidity characterization pyridine was used as probe molecule. The measurements in transmission mode were carried out on a Bruker Tensor 27 FTIR spectrometer equipped with a heatable and evacuable homemade reaction cell with CaF_2 windows connected to a gas-dosing and evacuation system. The sample powders were pressed into self-supporting wafers with a diameter of 20 mm and a weight of 50 mg. Before pyridine adsorption, the samples were pretreated by heating in synthetic air up to 673 K for 10 min, subsequent cooling to room temperature and evacuation. Pyridine was adsorbed at room temperature until saturation. Then the reaction cell was evacuated to remove physisorbed pyridine. The desorption of pyridine was followed by heating the sample in vacuum up to 673 K and recording spectra every 50 K. The spectra were measured with 2 cm^{-1} resolution and 64 scans.

2.3. Catalyst tests

All tests were performed in a 300 mL benchtop autoclave from Parr Instruments, equipped with a 40 mL catalyst stationary basket. Temperatures were maintained within ± 2 K from the target temperature. In a typical reaction, glycerol (>98%, Roth®) was used in aqueous solutions with a concentration of 10 wt%. Argon (Air Liquide 5.0) was used for drying the catalysts and to pressurize the autoclave in APR experiments, and hydrogen (Air Liquide 5.0) was used for catalyst pre-reduction and APH tests. Hydroxyacetone (90%, Sigma Aldrich) was used to prepare an aqueous solution for acetol hydrogenation. The setup used for catalyst pre-reduction and evaluation, the methodology for in situ pre-reduction and for the experiments are all described in detail in the Supplementary Information document.

The liquid phase products were analyzed by GC-FID (Shimadzu GC-17A) with autosampler (Chrompack FFAP column, 25 m × 0.32 mm × 0.3 µm), carrier He and 1,4-butanediol (99.9% from Sigma Aldrich) as internal standard. Initial method conditions were T = 313 K, p = 0.5 bar, v_{He} = 30 cm/s, split ratio = 50, and calibrations were done for glycerol, 1,2-PD, 1,3-PD, 1-PrOH, 2-PrOH, EG, acetone, acetol, ethanol, methanol, acetic acid, propionic acid, acrolein and allyl alcohol. The carbon balance in liquid phase was cross-checked with Total Organic Carbon analysis (TOC) using a TOC-V CPN equipment from Shimadzu. For product identification, GC-MS analysis was performed in a Shimadzu 2010 furnished with a CP-SIL 5 CB column (60 m × 0.32 × 8 µm). Gases were analyzed by an Agilent Technologies 7985A GC, equipped with TCD and FID detectors calibrated for permanent gases and hydrocarbons, furnished with CP Molsieve (25 m × 0.53 mm × 20µm) and PoraPLOT Q-HT (25 m × 0.53 mm × 20 µm) columns.

Glycerol conversion and selectivity were calculated on carbon basis. H_2 yield is defined as the percentage of produced H_2 moles over the initial quantity of glycerol moles in the feed solution, and the initial turnover frequency (TOF_0) was calculated using the number of active

Pt sites on the surface (Pt_{surf}) as obtained from chemisorption analysis. After the reaction, catalysts were separated from the solution using a magnet and filtered off, and the final solution was weighted and submitted to TOC analysis.

3. *Results and discussion*

3.1. Catalyst characterization

Table 1 shows the results from ICP analysis for each as-synthesized as well as spent platinum catalyst. The results indicate satisfactory impregnation of all the metals. Although $Al(HPO_3)_3$ was used for preparation of the solids, its contribution to the composition of the catalysts is negligible, and will thus be ignored in the discussion.

Texture and chemisorption results are available in Table 2. The samples show characteristic type II [20] isotherms corresponding to relatively small surface areas. The shape of the BET isotherms points to materials constituted mainly of separate particles with interstitial volume. BET area for the as-synthesized Fe_2O_3 support is similar to commercial Fe_2O_3 nanocat used as reference (32 m^2/g_{cat}). The reduction of the support causes a decrease in surface area, which remains stable during subsequent glycerol conversion. A much larger surface area drop from 160 to 16 m^2/g_{cat} was reported for high surface area-Fe_2O_3 used for dehydration and subsequent hydrogen transfer from glycerol to other products [12]. This fact is favors the presence of Pt particles over the synthesized support for catalyst stability regarding surface area.

Hydrogen chemisorption analysis was made for Fe_3O_4, 1.0Pt/Fe_3O_4 and 2.5Pt/Fe_3O_4 (Table 2). The tailor-made measurement protocol was used for the assessment of Pt particles, considering a correction for the hydrogen spillover phenomenon, since the amount of hydrogen uptake initially measured (1st and 2nd measures) was considerably larger than necessary for the impregnated amount of Pt. Previous tests revealed that only under vacuum

(10^{-2} mbar) at a reduction temperature of 523 K it was possible to remove efficiently all the chemisorbed hydrogen from partially reduced iron oxide support. The hydrogen spillover effect over Pt/Fe_3O_4 is responsible for the reduction of Fe_2O_3 to Fe_3O_4 in the presence of Pt at low temperatures [21,22], which is also discussed below along with the TPR results. As described in the experimental section, one of the hypotheses for the chemisorption methodology is that the hydrogen desorption energy for Pt particles differs from the desorption energy for sites where hydrogen atoms are spilled over, i.e., diffuse over the surface. It was also assumed that the flow of inert argon at the reduction temperature of the catalyst supplies enough energy to displace the hydrogen atoms attached only to the sites of lowest desorption energy, but not enough to displace hydrogen chemisorbed on the highest desorption energy sites.

The results revealed that these hypotheses were in accord with reality. Firstly, as seen in Table 2, there is no doubt that chemisorption occurs on the iron oxide support, but only in the presence of Pt particles, since no hydrogen uptake was measured for Fe_3O_4. The second interesting result was that the dispersion of Pt particles calculated from the 3rd chemisorption uptake for $1.0Pt/Fe_3O_4$ and $2.5Pt/Fe_3O_4$ perfectly agrees with literature [23,24] and with the particle sizes observed in the TEM results of this work (see below). Therefore, it is reasonable to state that the adsorption energy of the hydrogen atoms on the support Fe_3O_4 is higher than the adsorption energy on the active Pt metal particles. After correcting the spillover effect, catalysts $1.0Pt/Fe_3O_4$ and $2.5Pt/Fe_3O_4$ displayed metal dispersions and average particle sizes of 71% and 1.6 nm and 63% and 1.8 nm, respectively. The increase in Pt content causes a moderate drop in dispersion and little change in particle size. However, hydrogen spillover has a significant impact on catalytic activity, as discussed below. Figure 1 illustrates the steps and findings of the chemisorption methodology applied to quantify and correct the hydrogen spillover effect.

The procedure is not free from objections. For instance, the sample handling in order to evacuate bears the risk of exposing the reduced sample to atmospheric air, which can lead to deviations from real dispersion and particle size. However, this is possible for every *ex situ* reduction prior to characterization, but does obviously not seem to impede the procedure. Furthermore, the consistency of the particle diameters obtained from chemisorption (1.8 nm) and TEM studies (1.8 nm) is remarkable for 2.5Pt/Fe_3O_4. A second possible objection refers to the argon purge, asking whether the flow would be able to selectively remove the chemisorbed hydrogen from Pt species. Once again, the results justify the assumptions. The difference between the third uptake measure and the first two is larger than any difference between the first and the second uptake measures. If purging would remove all hydrogen, the third uptake measure should be the same as the second or slightly lower. Therefore three measurements were performed for each material. Nonetheless, there is some potential for improvement by flow adjustments and sample evacuation.

Figure 2 shows the TPR profiles for the Fe_2O_3 support and 2.5Ni/Fe_2O_3, 2.5Pd/Fe_2O_3, 1.0Pt/Fe_2O_3 and 2.5Pt/Fe_2O_3 catalysts. Table 3 displays the respective hydrogen uptake for reduction of the materials. In all profiles the hydrogen uptake is in agreement with the stoichiometry of the reduction of the support, $Fe_2O_3 + 3H_2 \rightarrow 2Fe + 3H_2O$. The excess of consumed H_2 in comparison to the calculated values suggests the reduction of oxychlorated artefacts from the impregnation process. The first peak in the reduction of Fe_2O_3 at 630 K was assigned to the transition $Fe_2O_3 \rightarrow Fe_3O_4$. , The first peak for the Pd and Pt catalysts comprehends the reduction of the active metals and the iron oxide transition (Table 3). Consequently, the active Pd and Pt catalysts reduced at 523 K are labeled as M/Fe_3O_4. Furthermore, the presence of group 10 metal shifts the support reduction to lower temperatures around 510 K, whereas only a slight shift can be observed for Ni. There are smooth and subtle humps around 430 K for Pt and Pd catalysts, which cannot be seen for

2.5Ni/Fe_2O_3. Hence, the reduction of Ni seems to occur first after Fe_2O_3 gets reduced. After the reduction of Pt or Pd, the chemisorbed hydrogen remains available on the active metal sites and diffuses to the surface of the support which is then reduced. According to literature [15,25-27], Pt/Fe_2O_3 and Pd/Fe_2O_3 have low reduction temperatures in agreement with our results. These low reduction temperatures are prerequisite for *in situ* pre-reduction in the autoclave due to allowed maximum temperature. It should be also noted that a low content of 1.0 wt% of Pt is sufficient to shift the transition $Fe_2O_3 \rightarrow Fe_3O_4$ to 510 K.

Figure 3 shows XRD patterns for as-synthesized Fe_2O_3, for calcined 2.5Pt/Fe_2O_3, for reduced 2.5Pt/Fe_3O_4, and for spent 2.5Pt/Fe_3O_4. The calcined Fe_2O_3 and 2.5Pt/Fe_2O_3 are shown in the lower part of the figure (a and b). The middle displays the patterns of the 2.5Pt catalysts after reduction at 423 K, 473 K and 523 K (c, d and e, respectively). The upper part presents the patterns for spent 2.5Pt/Fe_3O_4 (f and g). The patterns for the as-synthesized support and the calcined catalysts are similar to maghemite (γ-Fe_2O_3), which indicates that impregnation of Pt does not modify the lattice structure. No reflection for PtO_2 (for the calcined samples) or Pt (for the reduced samples) planes was observed, which is evidence for well dispersed particles, as corroborated by hydrogen chemisorption and TEM micrographs. Except for the 2.5Pt/Fe_2O_3 sample reduced at 423 K (c), all the reduced materials displayed in Figure 3 present patterns that match Fe_3O_4. This agrees with the TPR results for 2.5Pt/Fe_2O_3, and the conclusion that the transition $Fe_2O_3 \rightarrow Fe_3O_4$ can be shifted to 510 K only for the impregnated catalysts. Therefore, Fe_3O_4 is the actual support of the catalysts, since the *in situ* pre-reduction was done at 523 K. The spent 2.5Pt/Fe_3O_4 (f and g) catalysts' diffractograms also did not show any characteristic reflections for Pt planes, implying a stable state for the catalyst at the reaction temperature of 513 K.

Micrographs of Pt and Pd catalysts can be seen in Figures 4, 5 and 6, while Figures 7 and 8 show the metal particle size distribution for 2.5Pt/Fe_3O_4 and 1.0Pt/Fe_3O_4, respectively

The metal particles are shown in clear contrast and the elements were determined by EDX. From the TEM images, the Pt nanoparticles of 1.0Pt/Fe_3O_4 and 2.5Pt/Fe_3O_4 present dimensions similar to those obtained by hydrogen chemisorption. Figure 5a shows the lattice orientation of the support and the plane distance was measured as 0.295 nm, which is consistent with the interplanar distance of (220) planes of Fe_3O_4 [28]. The contrast obtained for 2.5Pd/Fe_3O_4 from TEM analysis was not as good as for the Pt catalysts, but the micrographs clearly indicate the existence of many Pd particles around 1 nm or even smaller (Figure 6a and b). However, the average metal particle size of 2.5Pd/Fe_3O_4 is notably larger than of Pt catalysts, since particles with diameters of 20 nm were found (Figure 6c). Assuming a gaussian distribution, the mean diameter for 2.5Pt/Fe_3O_4 is 1.56 nm ± 0.47 nm (Figure 7). The mean diameter for 1.0Pt/Fe_3O_4 was 0.77 ± 0.2 nm (Figure 8). These values are consistent with the chemisorption analysis (1.8 nm for 2.5Pt/Fe_3O_4) and with some values obtained from the literature (1.5 nm [13], 2.0 nm [15]).

Figures from the XP spectra can be found in the Supplementary Information document, alongside with details of the results. By contrasting the obtained results with the reference literature [29-50], it can be said the 2.5Pt catalyst shows a more stable reduction behavior than 2.5Pd, which is more stable than 2.5Ni. This order of reduction is in full agreement with the order of the catalyst activity. The XP spectra reveal that Pt particles are practically fully reduced prior to the reaction and are very mildly oxidized after the reaction, while Pd presents two distinct chemical states after reduction, and Ni is not reduced, even at 673 K, when there is a transformation from Fe_2O_3 to Fe_3O_4. The Fe_3O_4-supported particles are formed in such a way that Pt-Fe or Pd-Fe interactions stabilize adjacent Fe^{3+} and Fe^{2+} sites, which determine the overall dimensions of the particle and its d band energy. This effect is more pronounced in Pt catalysts, provided that Pt particles are smaller and more stable than Pd particles. This heterogeneous structure displays acid and basic sites, side by side with

nanoparticles that show a high potential to chemisorb glycerol and cleave its bonds by back donation. Acidity and basicity are considered to play an important role for the activity of the catalysts in APH of glycerol, and it has been recently reported that the impregnation of a noble metal increases greatly the acidity of the support [25]. From the changes in binding energies of the metals towards lower values after reduction, it follows that some acid-base properties of the catalyst should also be expected to alter after catalyst reduction. Active Lewis acid sites may interact with the lone electron pairs of oxygen atoms in hydroxyl groups, and Brønsted acid sites may protonate the hydroxyl, thereby catalyzing dehydration. In turn basic sites are able to dehydrogenate glycerol by means of electron donation to the hydrogen atom, thereby cleaving the O-H bond.

Temperature-programmed desorption of CO_2 (TPD) was undertaken to assess whether there is any relation between the catalysts' activity and their basic properties, and Figure 9 shows the results obtained for the materials. All materials possess basic sites with varying characteristics, and the impregnated metal enhances the support's basicity. Two peaks were found for the calcined Fe_2O_3, and their intensity substantially increased after reduction to Fe_3O_4 and by the addition of an active metal. By correlating the strength of the basic sites to the desorption temperature in a qualitative scale from weak (273-465 K), moderate (465-640 K) to strong (640-900 K) [26,51], the lower temperature peak is found around 570 K and ascribed to moderate basic sites, while strong basic sites generate signals at 680 K. As seen from Figure 9, the reduction of Fe_2O_3 to Fe_3O_4 increases the basicity of the material, which is mainly attributed to the presence of Fe^{2+} ions on the surface, which are able to donate electrons. The presence of Fe^{2+} on the surface agrees with the XPS results for Fe2p discussed above. 2.5Pd/Fe_3O_4 presents the largest number of moderate sites, and 2.5Ni/Fe_3O_4 has the overall largest number of basic and strongest sites. The signals of the strong basic sites are overlapped by tailing of the moderate sites for the 2.5Pt/Fe_3O_4 catalyst, and are seen as a

distinct shoulder for the 2.5Pd/Fe_3O_4 catalyst. Table 4 shows that the basic sites are a characteristic feature of the support, whereas the impregnated metals change the number of sites only to a limited extent. However, metal addition alters profoundly the nature of the basicity of the material. Compared to the Fe_3O_4 profile, Pt and Pd impregnation cause a decrease in the amount of strong basic sites, but generate an even higher amount of moderate sites, which does not happen for 2.5Ni/Fe_3O_4. On the contrary, Ni impregnation increases the number of strong basic sites. Since basic sites are already present in Fe_3O_4, and their number is lower than the molar quantity of impregnated metal, one can argue that the basicity stems from an effect the metals have on the support, rather than directly from the metallic sites. One possibility to explain the change in nature of the basic sites from Fe_3O_4 to 2.5Pt/Fe_3O_4 and 2.5 Pd/Fe_3O_4 is that Pt and Pd particles are formed on top of Fe^{2+} ions, therefore blocking them and in turn promoting milder sites on the particle-support interface.

Figure 10 shows the IR spectra for pyridine adsorption onto Fe_3O_4 and 2.5Pt/Fe_3O_4. For the presented spectra, wavenumbers around 1604 cm^{-1} and 1445 cm^{-1} indicate Lewis acid sites. The typical band of pyridine adsorption on Brønsted acid sites shows signals around 1540 cm^{-1} [52], which are missing in the measured spectra. The fact that the Brønsted acid sites are negligible on Fe_3O_4 is in agreement with studies on the nature of the acidity of iron oxide materials [53-55]. The presence of Brønsted sites on Fe_2O_3 is due to impurities [54], as is the case of SO_4^{2-} in the presence of an active metal like Mo, for example [55]. Although hydration of the support surface is expected to generate Brønsted acid sites in aqueous medium, it is likely to be in very limited extent. In light of the hydrogen chemisorption analysis, the present IR spectra indicate that the spillover effect does not generate protons on the surface of the support able to act as Brønsted sites. Although an absolute quantification of acid sites is difficult via IR spectroscopy, the absorbance for the Pt catalyst at 1445 cm^{-1} is

2.52 times more intense than the support's absorbance, clearly indicating that Pt impregnation increases the total number of Lewis acid sites.

3.2. Activity tests

The Weisz-Prater parameter was calculated using a glycerol diffusivity in water equal to 1.33×10^{-7} cm²/s, a tortuosity of 3.8, a porosity of 0.4 [56-61], and an average pore diameter of 14.3 nm as given by the physisorption analysis. The value was calculated to be $3.38 \times 10^{-2} << 1$,which suffices for kinetic assessment.

Table 5 shows conversions and selectivities for the Fe_3O_4-supported catalysts used in the APH of glycerol in regular batch experiments. All materials were submitted to *in situ* pre-reduction and 2.5Ni/Fe_3O_4 was reduced by means of a prior additional reduction step *ex situ* in a tubular oven under H_2 flow at 673 K. The results indicate that the platinum-based catalysts are best performing in APH among the used materials, even at lower Pt content, as is the case of 1.0Pt/Fe_3O_4 (81% conversion and 79.3% 1,2-PD selectivity), while 2.5Ni/Fe_3O_4 shows insatisfactory activity as well as low 1,2-PD selectivity. From a comparison of the obtained conversion results, the order of activity is very clear for the impregnated metals, namely, Ni < Pd < Pt. 1.0Pt/Fe_3O_4 led to promising results at 493 K at a mass ratio of $m_{glycerol}/m_{cat} = 10.4$. A recycle experiment was performed for 2.5Pt/Fe_3O_4, which showed considerable stability under the condition of excess water. In dry environments, using alcohols as hydrogen donors, the stability of iron oxide mixed with alumina as a support for Pt is noteworthy [16]. However, in the presence of hot water, Pt catalysts are known to suffer from deactivation processes such as leaching, sintering and acetol polymerization, in the cases involving glycerol dehydration [25,57].

Table 6 shows the activity and selectivity of the catalysts in the APR of glycerol, and once again 2.5Pt/Fe_3O_4 shows the highest conversion. However, 2.5Pd/Fe_3O_4 presents the best

performance in H_2 production (69.2% yield) and the highest selectivity towards 1,2-PD (45.3%). The same activity order as in APH is also found in APR: Pt > Pd > Ni. In comparison with results for Pd/Fe_2O_3 (conversion of 35% at 523 K, 15 g_{gly}/g_{cat} from ref. [26]), the conversion obtained in this work reaches the same range, using however a much lower amount of catalyst per batch (30 g_{gly}/g_{cat}), which seems to affect 1,2-PD selectivity, since in this work it was about 30%. In view of the fact that the APR of glycerol is mainly done for biomass valorization through H_2 production, it is useful to compare the results herein and the ones obtained for ethylene glycol by Huber et al. [17]. The results of this work confirm that Pd is more active for H_2 production, but there is a discrepancy in activity, since Pt was the most active in glycerol conversion. The interaction of the ethylene glycol molecules and the metal particles of Pd and Pt differs from the interaction of the glycerol molecules and the surface of the metal particles of these same metals, despite the similarities of the polyols. As it can be seen from the carbon balance in Table 6 (only calculated from liquid phase), there is considerable formation of CO_2 and hydrocarbons with $2.5Pt/Fe_3O_4$ and $2.5Pd/Fe_3O_4$. Although similar APR conversions were obtained for Fe_2O_3 and $2.5Ni/Fe_3O_4$, the H_2 yield was higher for the former. The main difference in H_2 yield from Pd to Pt is probably related to the ability of these metals to chemisorb hydrogen, which is more pronounced with Pd. Thus, hydrogen atoms on Pd particles combine faster and H_2 is released more easily than Pt surfaces.

The results displayed in Tables 4 to 6 evidence that the activity of the catalysts decreases when the number and strength of basic sites increases. Carbon monoxide was either absent or identified as trace in the analysis of the gas phase, which is due to water-gas shift reaction as an important part of the APR reaction network.

Further hydrogenolysis experiments with $2.5Pt/Fe_3O_4$ were made, since 1,2-PD yield was highest for this catalyst. Table 7 shows conversions, selectivities, carbon balances and

turnover frequencies for temperatures from 463 to 513 K, and Figure 11 shows the Arrhenius plot for APH using a first order apparent kinetic fit. Since hydrogen chemisorption studies indicated spillover, the turnover frequency was calculated using the third uptake measurement described herein, assuming a H/Pt_{surf} stoichiometry equal to one. The turnover frequencies for $2.5Pt/Fe_3O_4$ are comparable to the previously presented Pt_xFe_y/Al_2O_3 catalysts [19]. Apparent activation energy of 61.1 kJ/mol was obtained, which is slightly lower than for ruthenium catalysts [58], which also agrees with the value of 63.7 kJ/mol obtained by Jin et al. for Pt/C [59].

Hydrogen partial pressure is important as it controls solubility and concentration near the catalyst surface and thus can influence both reforming and hydrogenolysis. It has been reported that H_2 pressures as low as 3.4 bar are enough to drive hydrogenolysis at 473 K with 25% conversion [60]. It is also known that H_2 solubility drops drastically as glycerol concentration is increased [61]. For low glycerol concentrations, as used throughout this work (10 wt%), there is very little difference from the solubility of H_2 in pure water [61-63], Table 8 shows the pressure impact on $2.5Pt/Fe_3O_4$ performance in *regular batch* experiments, and Figure 12 shows the behavior of the reaction for two *constant pressure batch* experiments. Higher pressures cause considerable loss in conversion without increasing 1,2-PD selectivity significantly (Table 8).

As expected, acetol selectivity decreases with higher H_2 pressures because of carbonyl hydrogenation. The gauge water vapor pressure at 493 K can be estimated to approximately 25 bar. Therefore, in Figure 12, at a total pressure of (i) 35 bar, the H_2 partial pressure is 10 bar, while at a total pressure of (ii) 60 bar, the H_2 partial pressure is 35 bar. The total pressure was maintained constant throughout the entire reaction, and 1,2-PD selectivity stabilizes after some time. Although both experiments displayed in Figure 12 showed similar initial conversions at t_0 – (i) 5.8%, and (ii) 6.0%, due to glycerol consumption in APR and

dehydrogenation processes prior to hydrogen uptake – they end up with different conversions after four hours: (i) 17.5%, and (ii) 13.5%. Since 1,2-PD selectivity remains fairly stable and its increase accompanies the acetol selectivity decrease, this is proof that acetol is being consumed to form 1,2-PD. The only difference between the conditions of the experiments (i) and (ii) is the pressure value, and therefore lower conversions obtained for high H_2 pressure indicate that some step in 1,2-PD formation is hindered by the hydrogen excess. Since acetol hydrogenation consumes H_2, it is likely that the decrease in conversion observed when more hydrogen is available ensues from a dehydrogenation prior to acetol production.

The decrease in conversion caused by the increase in hydrogen pressure does not agree with Le Châtelier's principle, and, therefore, it has to be a kinetic effect. For the present Pt catalyst, there are two main explanations for this phenomenon. The first one is that hydrogen spillover occurs on the surface of the catalyst. Therefore, increasing hydrogen pressures cause increasing active site blockage on the catalyst surface as a whole. This blockage impedes the interaction of glycerol and the catalyst surface and slows down the reaction. The second explanation stems from the reaction mechanism, since APR reactions show that H_2 is produced from glycerol conversion.

As seen in Figure 13, there are at least three well accepted mechanisms for 1,2-PD production from glycerol over noble metals, [60,64-71] namely (a) the dehydration-hydrogenation route [60], (b) the dehydrogenation-dehydration-hydrogenation route [65-68] and (c) the direct hydrogenolysis route [69,70]. Acetol is an intermediate in the production of 1,2-PD, and its formation is accepted to run via an enol-keto tautomerization mechanism during glycerol dehydration over Lewis acid sites [64,72], while acrolein, which is also a product from the dehydration of glycerol, is thought to be produced over Brønsted acid sites. As reported elsewhere [66], the formation of 1,2-PD via preceding dehydrogenation over metal sites is more likely than from a first dehydration catalyzed by acid sites. Despite their

acidic properties, acetol is not produced when only a bare oxide is used, such as CeO_2, La_2O_3, ZnO [25], TiO_2 [73] and Al_2O_3 [74]. This poor dehydration activity coupled with the observed dehydrogenation strongly suggests that metallic and acid functions are required in the typical temperature range of hydrogenolysis (453-523 K). The very low selectivity for 1,3-PD in our APH and APR experiments is also evidence that a Brønsted acid catalyzed protonation of the secondary hydroxyl is unlikely to occur over the iron oxide-supported catalysts. The order of metal activity, Pt > Pd > Ni, both with and without external H_2, shows that steps in the production of acetol are deeply connected with the bifunctional ability of the metal sites to dehydrate and dehydrogenate glycerol.

Thus, for the present catalysts, the dehydration-hydrogenation mechanism (a) explains the formation of acetol, but does not satisfactorily clarify the negative effect of hydrogen pressure increase on the conversion. It requires additional explanation about the responsible sites for the initial protonation, since pyridine adsorption IR spectroscopy revealed no Brønsted acid sites. Moreover, acetol hydrogenation was tested over Fe_2O_3 at 493 K, and although conversion was high (79%for a 10 wt% aqueous solution with 0.5 g of Fe_2O_3 at 20 bar H_2), 1,2-PD selectivity was very poor (25%) with formation of a final mixture comprising two phases. This means that acetol hydrogenation is not the main reaction path towards 1,2-PD, as also pointed out in [25].

By means of GC-MS analysis of the APR reaction products, traces of epoxides like glycidol and oxirane-methoxymethyl were found among other compounds. Moreover, when exposed to ambient air for few hours, the final solution changes from colorless to a yellow reddish mixture, indicating that albeit the small concentration, unstable products are present. It has been reported that glycerol is converted into epoxides with considerable selectivity over Ni/γ-Al_2O_3 [75]. Glycidol should be expected to be unstable in the reaction medium with water excess and easily hydrogenated to 1,2-PD. Part of the dehydrogenation processes in the

initial steps may also occur, in a low extent, via epoxide formation. At this point it should be noted that none of the aforementioned mechanisms addresses the formation of epoxides.

As observed in the experiments with varying H_2 pressure over 2.5Pt/Fe_3O_4, increasing the pressure does not accelerate the reaction rate, probably due to site blockage. This means the site availability has a pronounced effect in the reaction rate. From another perspective, many papers on Langmuir-Hinshelwood Hougen-Watson mechanism show that a high adsorption constant for H_2 could explain the drop in conversion caused by hydrogen pressure increase [59,76-79]. This can also be connected to the hydrogen spillover. The low selectivity towards 1,3-PD in comparison to 1,2-PD can be due to the nature of the active acid sites in the present catalysts. For instance, the reduction of WO_3 produces H_xWO_3, which are typical Brønsted acids, and these materials are used as supports of catalysts for the production of 1,3-PD from glycerol [80-82]. On the other hand, the reduction of Fe_2O_3 to Fe_3O_4 increases the number of basic sites (Figure 9), as well as the number of Lewis acid sites (Figure 10). Thus, although spillover occurs and the hydrogen transport could likely lead to the formation of protons on the surface, the catalyst activity is a function of the Lewis acid sites. Therefore, although the presence of active hydrogen is indispensable to the hydrogenation steps, it inhibits the activation of the glycerol molecule in the slow steps of dehydrogenation and dehydration.

It has been recently shown that incorporation of Pt increases the acidity of different supports, causing an effect in catalyst activity towards glycerol hydrogenolysis [25], which is corroborated by the pyridine adsorption analysis in the present work. It is shown herein that basicity is also greatly affected by metal impregnation, and since dehydrogenation seems to be a crucial step prior to the formation of 1,2-PD, Lewis acid sites and basic sites play a role in activity. Lewis acid sites on the particles can thus interact with the oxygen atoms in hydroxyl groups of glycerol while neighbor active metal atoms can further chemisorb the

hydrogen atom from the hydroxyl and from the terminal carbon acting as bases. The ability of the impregnated metal to form stable reduced active particles at the reduction conditions is crucial to activity, and depends on intrinsic characteristics of the element. For the present catalysts, metal reducibility follows the order: Pt > Pd > Ni, as observed from XPS results, which is the same order of the catalysts' activity. However, it should be noted that under more controlled conditions of reduction, model surfaces of Ni could perform as better catalysts then the presently portrayed.

A straightforward interpretation of the connection between basicity and catalytic activity is not clear. It can be said that the catalysts with higher activity are also the ones possessing the lowest amount of strong basic sites and largest amount of moderate basic sites. However, in view of the results, it is not possible to state that strong basic sites cause a poor catalyst activity. Further experiments with extra iron oxide-supported materials should be undertaken with different proportions of basic sites in order to check for an unequivocal relationship between basic sites and their effect on APH or APR. From TEM analysis, Pt presents smaller particles than Pd, which is evidence that smaller particles have a positive effect on catalyst activity. It is important to note that in our previous work on Pt_x-Fe_y/Al_2O_3 [19] it was found that larger Pt-Fe particles were more active. This apparent contradiction is probably due to the absence of reduced bimetallic Pt-Fe particles in the present work, since the reduction temperatures used in the present experiments were lower. Thus, overlayers of Fe^0 over the Pt particles are less likely to occur, favoring smaller particles.

Particle size plays an important role in hydrogenolysis reactions, considered sensitive to the structure of the catalyst [83]. Albeit the different activity, 1,2-PD selectivity does not change much from 2.5Pd/Fe_3O_4 to 2.5Pt/Fe_3O_4, which means that hydrogenation steps occur more easily than dehydrogenation on the particles of both metals. Recent studies reveal that dehydrogenation of hydrocarbons on Pt surfaces is favored by small particles [84,85], and

therefore, a particle distribution with larger Pd particles seems to explain in part its lower catalyst activity. The case is not inverse for APR, but it is different, due to the dissimilar desorption energies of H_2 on the surface of Pd and Pt particles. Given the smaller average particle diameter of Pt particles, a larger number of active sites is expected to dehydrogenate the glycerol molecules on 2.5Pt/Fe_3O_4 than on 2.5Pd/Fe_3O_4, hence the higher conversion of the former.

4. Conclusions

Glycerol hydrogenolysis and APR share some of the same reaction steps, which necessarily include dehydrogenation as the initial interaction between glycerol and the metallic nanoparticles. The Fe_3O_4-supported Pt, Pd and Ni catalysts vary remarkably in activity, according to the impregnated metal, but all materials studied presented some activity. Moreover, the fact that Fe_2O_3 is active at the low reaction temperature of 503 K, is highly interesting for APR reactions conducted at higher temperatures aiming at H_2 production, given the fact that Fe_2O_3 presents virtually no cost-related issues in comparison to other materials. As shown by XRD analysis of spent Pt containing catalysts, when used as support for this metal, Fe_3O_4 does not present the drawback of being structurally changed by hydration, as for example γ-Al_2O_3, which is transformed into boehmite [57].

The formation of stable reduced metallic particles seems to be the greatest limiting feature of the presented catalysts for the reaction. Further studies with higher reduction temperatures, especially for as-synthesized Ni/Fe_2O_3 catalysts, may show promise, since support phase transition from Fe_3O_4 to FeO is expected to occur as well as metallic particle formation. The *in situ* pre-reduction setup seems to be well suited for hydrogenolysis and APR batch reactions, having the limitation of being only suitable for catalysts with low reduction temperature, such as the case of supported Pt and Pd. After reduction of the catalyst, the

change in the support composition, from Fe_2O_3 to Fe_3O_4, in tandem with the presence of Pt and Pd active as nanoparticles, has a profound effect in the acid-base characteristics of the catalyst, as well as in the hydrogen uptake and spillover ability. For the Pt catalyst, the H_2 spillover is likely the cause of the drawback in conversion for high hydrogen pressures. The best performing catalyst for hydrogenolysis, 2.5Pt/Fe_3O_4, remains stable even after the reaction, and the conversion drop in catalyst recycle is relatively low. As an additional advantage for batch operation, it should be highlighted that the Fe_3O_4-supported materials can be (and actually were) separated from the reaction solution using a magnet, which is highly desirable for catalyst recovery.

5. *Acknowledgements*

The Brazilian authors would like to thank CAPES , CNPq and FAPERJ. The authors would also like to thank all the colleagues in the analytical department of LIKAT.

References

[1] R. Connor, H. Adkins, *J. Am. Chem. Soc.* 54 (1932) 4678-4690.

[2] R.R. Davda, J.W. Shabaker, G.W. Huber, R.D. Cortright, J.A. Dumesic, *Appl. Catal. B* 43 (2003) 13-26.

[3] A.V.H. Soares, J.B. Salazar, D.D. Falcone, F.A. Vasconcellos, R.J. Davis, F.B. Passos, *J. Mol. Catal. A Chem.* 415 (2016) 27-36.

[4] A. Pamphile-Ádrian, P.P. Florez-Rodriguez, F.B. Passos, *J. Braz. Chem. Soc.* 27 (2016) 958-966.

[5] L. Yin, D. Chen, M. Feng, L. Ge, D. Yang, Z. Song, B. Fan, R. Zhang, G. Shao, *RSC Adv.* 5 (2015) 328-337.

[6] D. Lee, Y.-W. Choi, Y.-S. Na, S.-S. Choi, D.-W. Park, J. Choi, *Mat. Res. Bull.* 68 (2015) 221-226.

[7] W. Cheng, J. Xu, Y. Wang, F. Wu, X. Xu, J. Li, *J. Colloid Interface Sci.* 445 (2015) 93-101.

[8] R. Li, Y. Jia, N. Bu, J. Wu, Q. Zhen, *J. Alloys Compd.* 643 (2015) 88-93.

[9] D.E. Stobbe, F.R. van Buren, A.W. Stobbe-Kreemers, J.J. Schokker, A.J. van Dillen, J.W. Geuss, *J. Chem. Soc. Faraday Trans.* 87 (1991) 1623-1629.

[10] D.E. Stobbe, F.R. van Buren, A.J. van Dillen, J.W. Geuss, *Stud. Surf. Sci. Catal*. 75 (1993) 2337-2340.

[11] D.R. Milburn, K.V.R. Chary, R.J. Obrien, B.H. Davis, *Appl. Catal. A* 144 (1996) 133-146.

[12] Y. Liu, H. Tuysuz, C.-J. Jia, M. Schwickardi, R. Rinaldi, A.-H. Lu, W. Schmidt, F. Schüth, *Chem. Commun*. 46 (2010) 1238-1240.

[13] S. Kang, P.K. Shen, *Electrochim. Acta* 168 (2015) 104-110.

[14] X. Xu, T. Liu, P. Xie, Y. Yue, C. Miao, W. Hua, Z. Gao, *Catal. Comm*. 54 (2014) 77-80.

[15] N. An, P. Wu, S. Li, M. Jia, W. Zhang, *Appl. Surf. Sci*. 285 (2013) 805-809.

[16] E.S. Vasiliadou, A.A. Lemonidou, *Catalysts* 4 (2014) 397-413.

[17] G.W. Huber, J.W. Shabaker, S.T. Evans, J.A. Dumesic, *Appl. Catal. B* 62 (2006) 226-235.

[18] J. Lee, Y.T. Kim, G.W. Huber, *Green Chem*. 16 (2014) 708-718.

[19] A.V.-H. Soares, P. Geronimo, F.B. Passos, *Appl. Catal. B*, 185 (2016) 77-87.

[20] K.S.W. Sing, *Pure Appl. Chem.* 54 (1982) 2201-2218.

[21] G. Fröhlich, W.M.H. Sachtler, *J. Chem. Soc. Faraday Trans*. 94 (1998) 1339-1346.

[22] H.-Y. Liu, W.-A. Chiou, G. Fröhlich, W.M.H. Sachtler, *Top. Catal*. 10 (2000) 49-57.

[23] B.J. Kip, F.B.M. Duivenvoorden, D.C. Koningsberger, R. Prins, *J. Am. Chem. Soc*. 108 (1986) 5633-5634.

[24] G.C. Bond, *Platin. Met. Rev.*19 (1975) 126-134.

[25] M. Checa, A. Marinas, J.M. Marinas, F.J. Urbano, *Appl. Catal. A*. 507 (2015) 34-43.

[26] J. Ge, Z. Zeng, F. Liao, W. Zheng, X. Hong, S.C.E. Tsang, *Green Chem*. 15 (2013) 2064-2069.

[27] F. Mauriello, A. Vinci, C. Espro, B. Gumina, M.G. Musolino, R. Pietropaolo, *Catal. Sci. Tech*. 5 (2015) 4466-4473.

[28] J. Li, H. Zeng, S. Sun, J.P. Liu, Z.L.Wang, *J. Phys. Chem. B* 108 (2004) 14005-14008.

[29] V.I. Nefedov, Y.V. Salyn, G. Leonhardt, R. Scheibe, *J. Elec. Spec. Rel. Phenom*. 10 (1977) 121-124.

[30] P. Mills, J.L. Sullivan, *J. Phys. D Appl. Phys*. 16 (1983) 723-732.

[31] E. Paparazzo, *J. Elec. Spec. Rel. Phenom*. 43 (1987) 97-112.

[32] D. Brion, *Appl. Surf. Sci*. 5 (1980) 133-152.

[33] G.C. Allen, M.T. Curtis, A.J. Hooper, P.M. Tucker, *J. Chem. Soc. Dalton Trans.* 14 (1974) 1525-1530.

[34] N.S. McIntyre, D.G. Zetaruk, *Anal. Chem*. 49 (1977) 1521-1529.

[35] G.M. Bancroft, I. Adams, L.L. Coatsworth, C.D. Bennewitz, J.D. Brown, W.D. Westwood, *Anal. Chem*. 47 (1975) 586-588.

[36] J.P. Contour, G. Mouvier, M. Hoogewys, C. Leclere, *J. Catal*. 48 (1977) 217-228.

[37] T.H. Fleisch, G.J. Mains, *J. Phys. Chem*. 90 (1986) 5317-5320.

[38] T.H. Fleisch, G.W. Zajac, J.O. Schreiner, G.J. Mains, *Appl. Surf. Sci*. 26 (1986) 488-497.

[39] E. Janin, M. Björkqvist, T.M. Grehk, M. Götheld, C.M. Pradier, U.O. Karlsson, A. Rosengren, *Appl. Surf. Sci*. 99 (1996) 371-378.

[40] J.E. Drawdy, G.B. Hoflund, S.D. Gardner, E. Yngvadottir, D.R. Schryer, *Surf. Interface Anal*. 16 (1990) 369-374.

[41] M. Alnot, V. Gorodetskii, A. Cassuto, J.J. Ehrhardt, *Thin Solid Films* 151 (1987) 251-262.

[42] C. Battistoni, A.M. Giuliani, E. Paparazzo, F. Tarli, *J. Chem. Soc. Dalton Trans.* 7 (1984) 1293-1299.

[43] C. Sleigh, A.P. Pijpers, A. Jaspers, B. Coussens, R.J. Meier, *J. Elec. Spec. Rel. Phenom*. 77 (1996) 41-57.

[44] A. Tressaud, S. Khairoun, H. Touhara, N. Watanabe, *Z. Anorg. Allg. Chem*. 540 (1986) 291-299.

[45] J.M. Tura, P. Regull, L. Victori, M.D. De Castellar, *Surf. Interface Anal*. 11 (1988) 447-449.

[46] K.S. Kim, N. Winogard, *Surf. Sci*. 43 (1974) 625-643.

[47] R.B. Shalvoy, P.J. Reucroft, B.H. Davis, *J. Catal*. 56 (1979) 336-348.

[48] T. Dickinson, A.F. Povey, P.M.A. Sherwood, *J. Chem. Soc. Faraday Trans. 1* 73 (1977) 327-343.

[49] S.O. Grim, L.J. Matienzo, W.E. Swartz, *J. Am. Chem. Soc*. 94 (1972) 5116-5117.

[50] A.B. Mandale, S. Badrinarayanan, S.K. Date, A.P.B. Sinha, *J. Elec. Spec. Rel. Phenom*. 33 (1984) 61-72.

[51] H. Hattori, *J. Jpn. Pet. Inst*. 47 (2004) 2.

[52] E.P. Parry, *J. Catal*. 2 (1963) 371-379.

[53] G. Busca, V. Lorenzelli, *Mat. Chem*. 6 (1981) 175-185.

[54] V. Lorenzelli, G. Busca, *Mat. Chem. Phys*. 13 (1985) 261-281.

[55] M.M. Mohamed, B.M. Abu-zied, *Thermochim. Acta* 359 (2000) 109-117.

[56] S.R. Fogler, *Elementos de Engenharia das Reações Químicas.* 3rd Edition, LTC, Rio de Janeiro, 2002, p. 697.

[57] R.M. Ravenelle, F.Z. Diallo, J.C. Crittenden, C. Sievers, *ChemCatChem* 4 (2012) 492-494.

[58] D.G. Kovacs, J.E. Jackson, D.J. Miller, *Abst. Papers Am. Chem. Soc.*, San Diego, CA, 1-6 april, 2001, v. 221, p. U177-U178, Part 2. Abstract 457-ORGN.

[59] X. Jin, B. Subramaniam, R.V. Chaudhari, P.S. Thapa, *AIChE J.* 62 (2016) 1162-1173.

[60] M.A. Dasari, P.-P. Kiatsimkul, W.R. Sutterlin, G.J. Suppes, *Appl. Catal. A* 281 (2005) 225-231.

[61] Physical Properties of Glycerine and its solutions, Hydrocarbon Process. 1967. < http://www.aciscience.org/docs/physical_properties_of_glycerine_and_its_solutions.pdf>.

[62] T.E. Crozier, S. Yamamoto, *J. Chem. Eng. Data* 19 (1974) 242-244.

[63] H.A. Pray, C.E. Schweickert, B.H. Minnich, *Ind. Eng. Chem*. 44 (1952) 1146-1151.

[64] A. Martin, U. Armbruster, I. Gandarias, P.L. Arias, *Eur. J. Lipid Sci. Tech*. 115 (2013) 9-27.

[65] C. Montassier, J.C. Ménézo, L.C. Hoang, C. Renaud, J. Barbier, *J. Mol. Catal*. 70 (1991) 99-110.

[66] A. Alhanash, E.F. Kozhenikova, I.V. Kozhenikov, *Catal. Lett*. 120 (2008) 307-311.

[67] E.P. Maris, R.J. Davis, *J. Catal*. 249 (2007) 328-337.

[68] E.P. Maris, W.C. Ketchie, M. Murayama, R.J. Davis, *J. Catal*. 251 (2007) 281-294.

[69] Y. Nakagawa, Y. Shinmi, S. Koso, K. Tomoshige, *J. Catal*. 272 (2010) 191-194.

[70] Y. Shinmi, S. Koso, T. Kubota, Y. Nakagawa, K. Tomishige, *Appl. Catal. B* 94 (2010) 318-326.

[71] H. Atia, U. Armbruster, A. Martin, *Appl. Catal. A* 393 (2011) 331-339.

[72] A. Alhanash, E.F. Kozhevnikova, I.V. Kozhevnikov, *Appl. Catal. A* 378 (2010) 11-18.

[73] J.B. Salazar, D.D. Falcone, H.N. Pham, A.K. Datye, F.B. Passos, R.J. Davis, *Appl. Catal. A* 482 (2014) 137-144.

[74] X. Lin, Y. Lv, Y. Xi, Y. Qu, D.L. Phillips, C. Liu, *Energ. Fuels* 28 (2014) 3345-3351.

[75] P.P. Florez-Rodriguez, A.J. Pamphile-Adrián, F.B. Passos, *Catal. Today* 237 (2014) 38-46.

[76] A. Torres, D. Roy, B. Subramaniam, R.V. Chaudhari, *Ind. Eng. Chem. Res*. 49 (2010) 10826-10835.

[77] Y. Xi, J.E. Halladay, J.G. Frye, A.A. Oberg, J.E. Jackson, D.J. Miller, *Org. Process Res. Dev*. 14 (2010) 1304-1312.

[78] Z. Zhou, X. Li, T. Zeng, W. Hong, Z. Cheng, W. Yuan, *Chin. J. Chem. Eng*. 18 (2010) 384-390.

[79] R.V. Sharma, P. Kumar, A.K. Dalai, *Appl. Catal. A* 477 (2014) 147-156.

[80] S. Zhu, X. Gao, Y. Zhu, Y. Li, *J. Mol. Catal. A* 398 (2015) 391-398.

[81] S. García-Fernández, I. Gandarias, J. Requies, M.B. Güemez, S. Bennici, A. Auroux, P.L. Arias, *J. Catal*. 323 (2015) 65-75.

[82] J. Wang, X. Zhao, N. Lei, L. Li, L. Zhang, S. Xu, S. Miao, X. Pan, A. Wang, T. Zhang, *ChemSusChem* 9 (2016) 784-790.

[83] J.H. Sinfelt, J.L. Carter, D.J.C. Yates, *J. Catal*. 24 (1972) 283-296.

[84] Y. Chu, Q. Zhang, T. Wu, Z. Nawaz, Y. Wang, F. Wei, *J. Nanosci. Nanotech*. 14 (2014) 6900-6906.

[85] J. Zhu, M.-L. Yang, Y. Yu, Y.-A. Zhu, Z.-J. Sui, X.-G. Zhou, A. Holmen, D. Chen, *ACS Catal*. 5 (2015) 6310-6319.

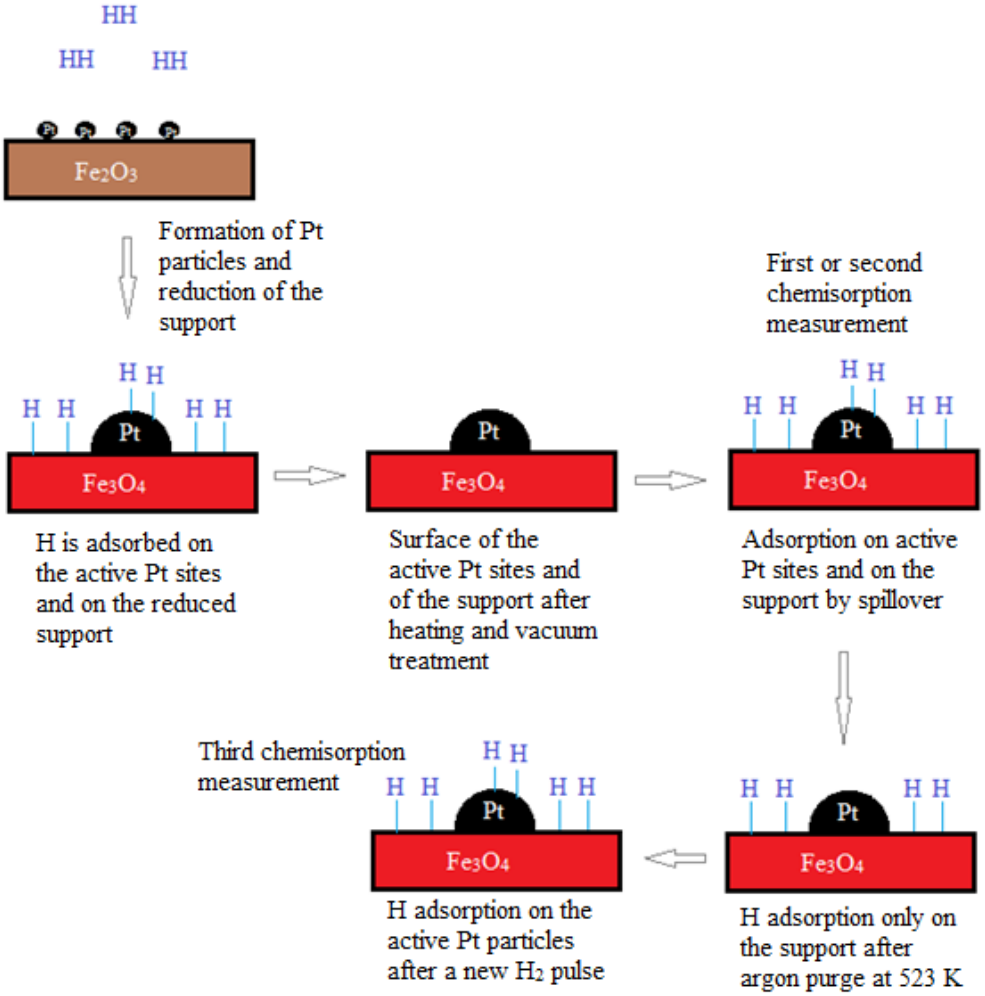

Figure 1: Scheme for the hydrogen chemisorption analysis to measure Pt dispersion on Fe_3O_4 particles with consideration of the spillover effect.

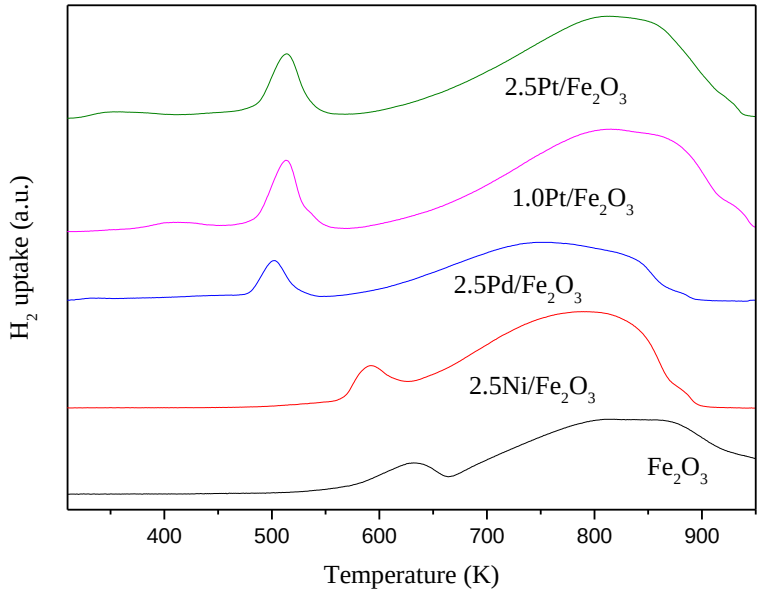

Figure 2: TPR profiles for Fe_2O_3 (support), 2.5Ni/Fe_2O_3, 2.5Pd/Fe_2O_3, 1.0Pt/Fe_2O_3 and 2.5Pt/Fe_2O_3.

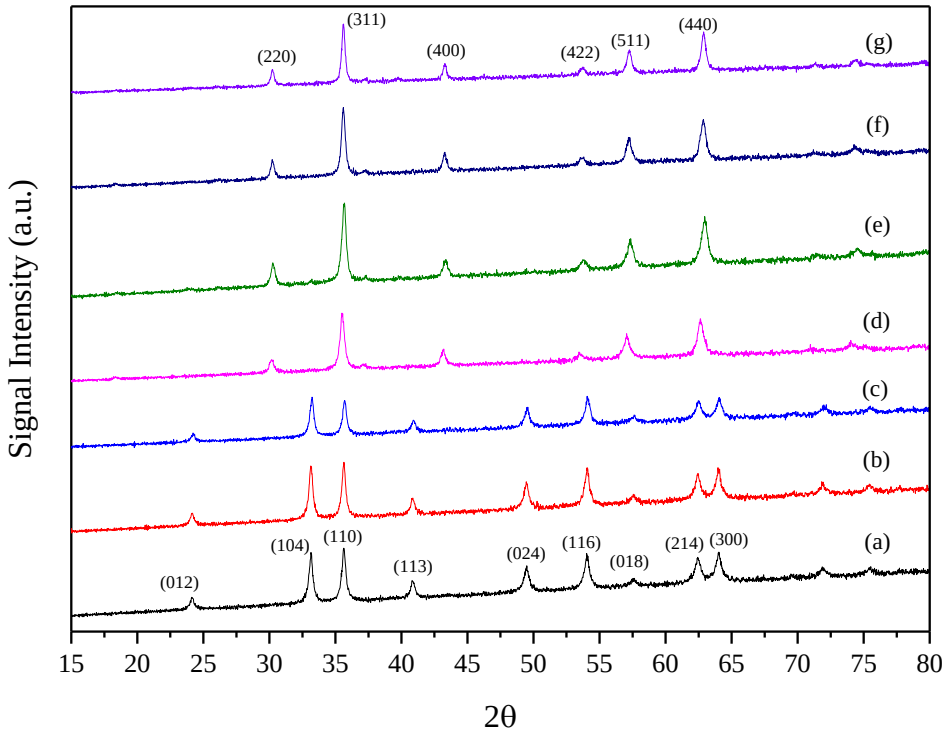

Figure 3: XRD patterns for (a) as-synthesized Fe_2O_3, (b) calcined 2.5Pt/Fe_2O_3, (c) 2.5Pt/Fe_2O_3 reduced at 423 K, (d) 2.5Pt/Fe_3O_4 reduced at 473 K, (e) 2.5Pt/Fe_3O_4 reduced at 523 K, (f) 2.5Pt/Fe_3O_4 after APH at 473 K, (g) 2.5Pt/Fe_3O_4 after APH at 513 K.

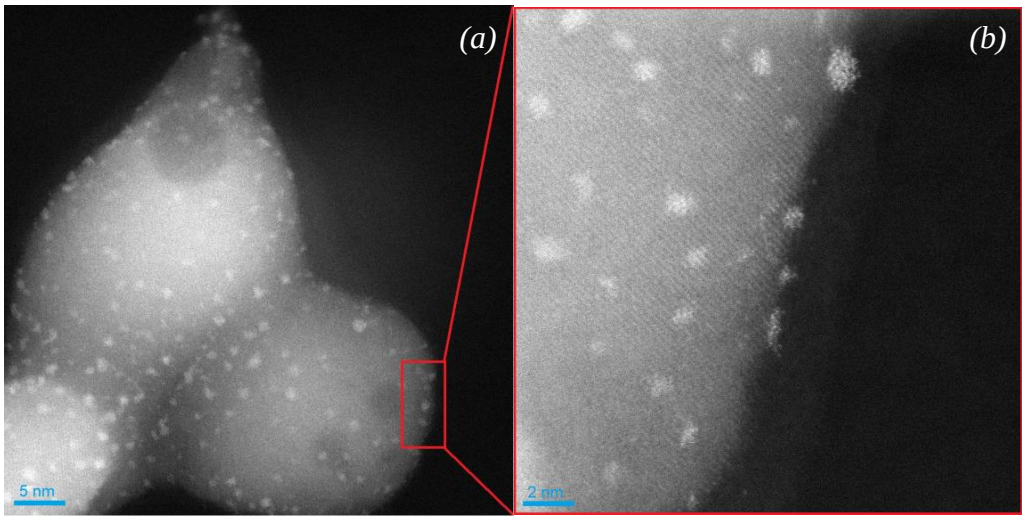

Figure 4: TEM micrographs of catalyst 1.0Pt/Fe_3O_4.

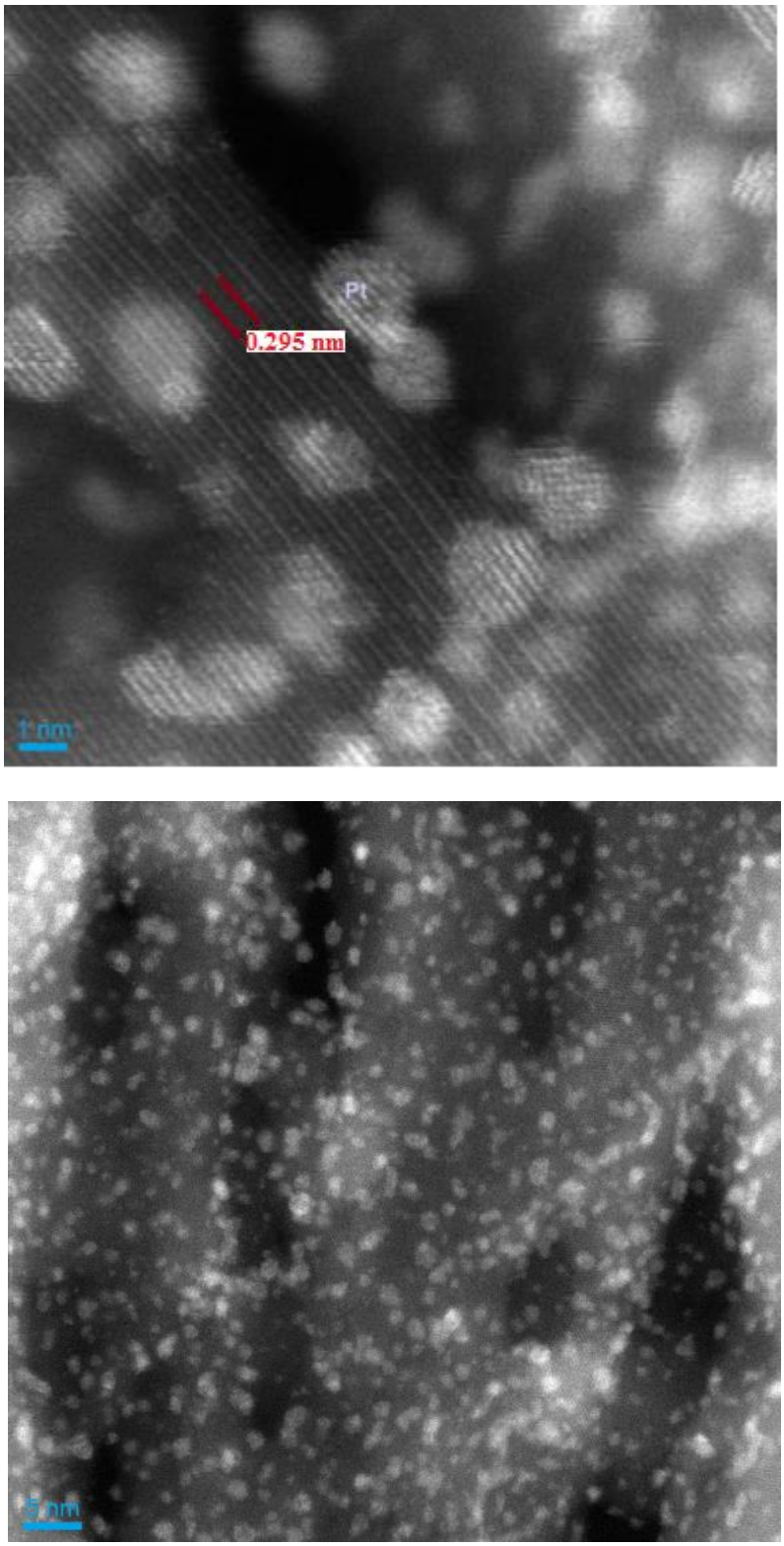

Figure 5: TEM micrographs of 2.5Pt/Fe_3O_4. (a) used to identify the interplanar lattice distance from the plane (220) of the support Fe_3O_4. (b) the particle dispersion.

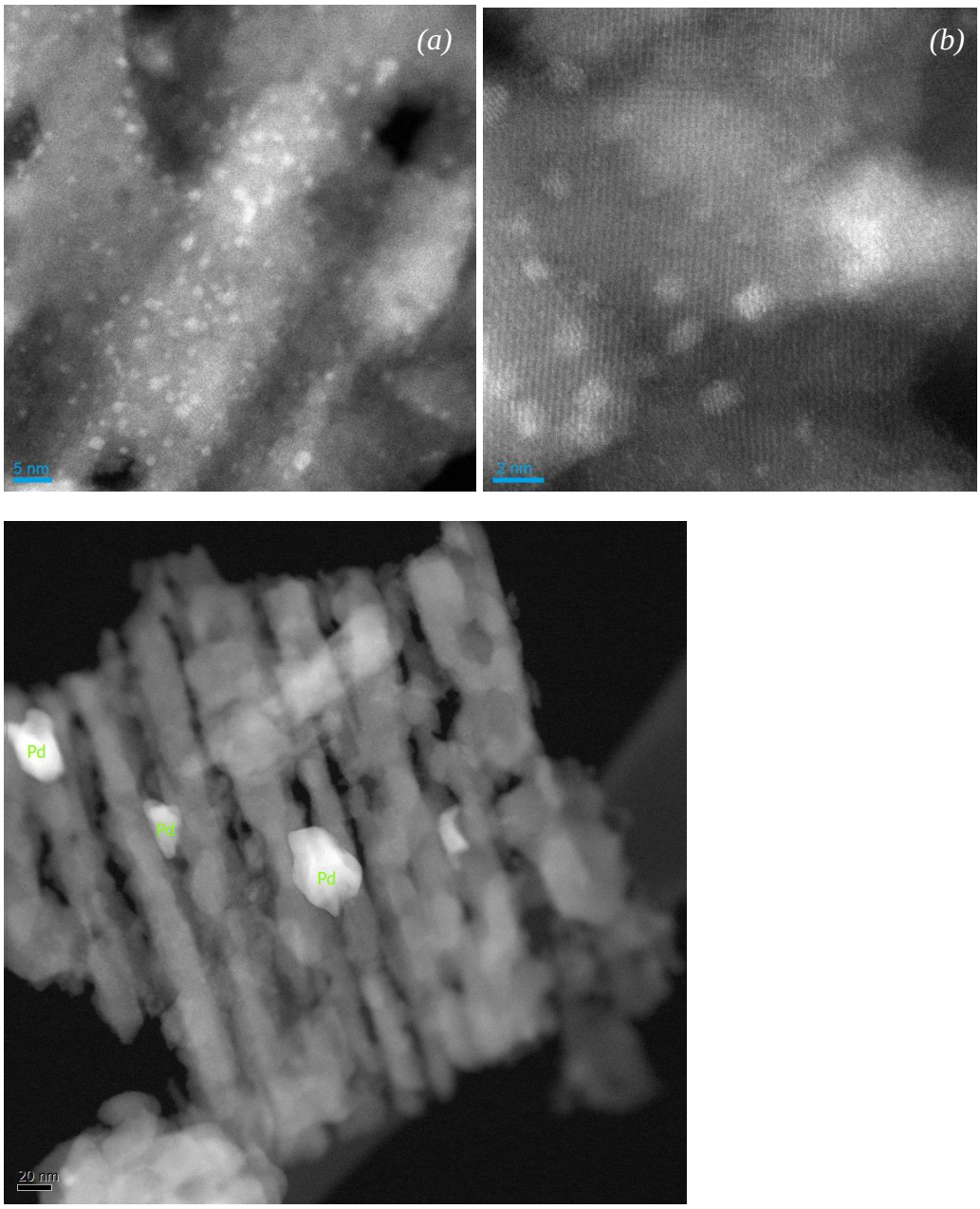

Figure 6: TEM micrographs of 2.5Pd/Fe_3O_4. (a) and (b) show dispersed nanoparticles with diameters below 1 nm, (c) features Pd particles with diameters exceeding 20 nm.

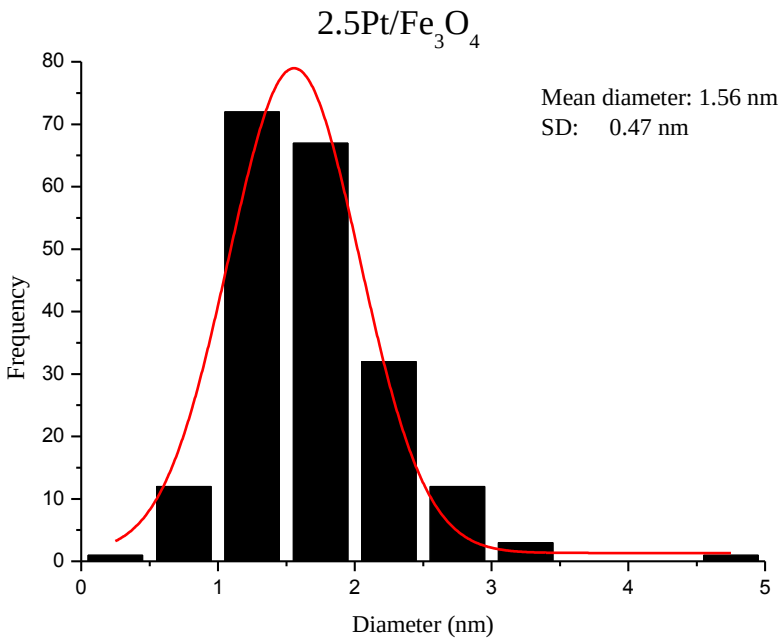

Figure 7: Metal particle size distribution for $2.5Pt/Fe_3O_4$.

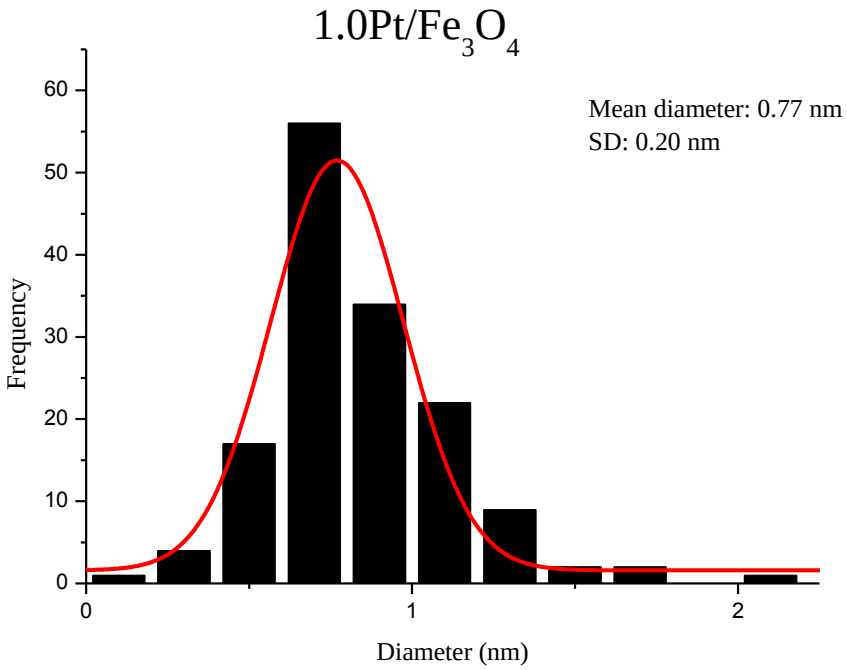

Figure 8: Metal particle size distribution for 1.0Pt/Fe_3O_4.

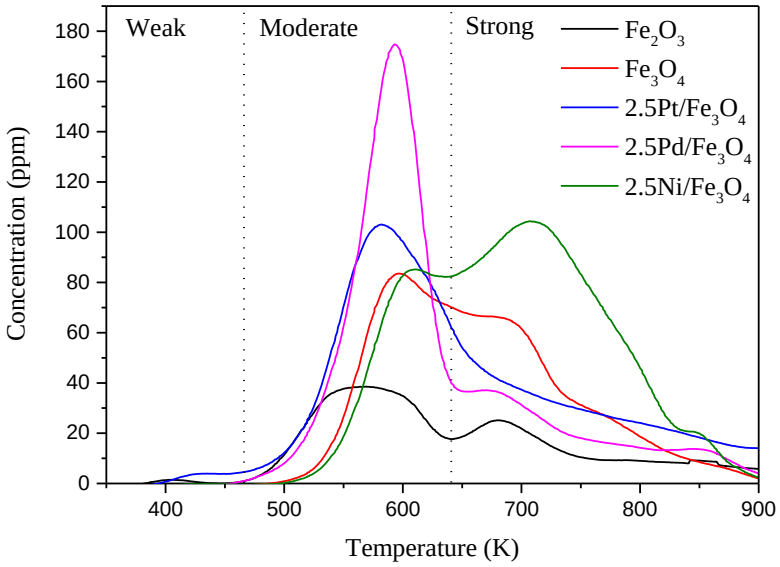

Figure 9: CO_2 TPD results for Pt, Pd and Ni catalysts supported on iron oxide.

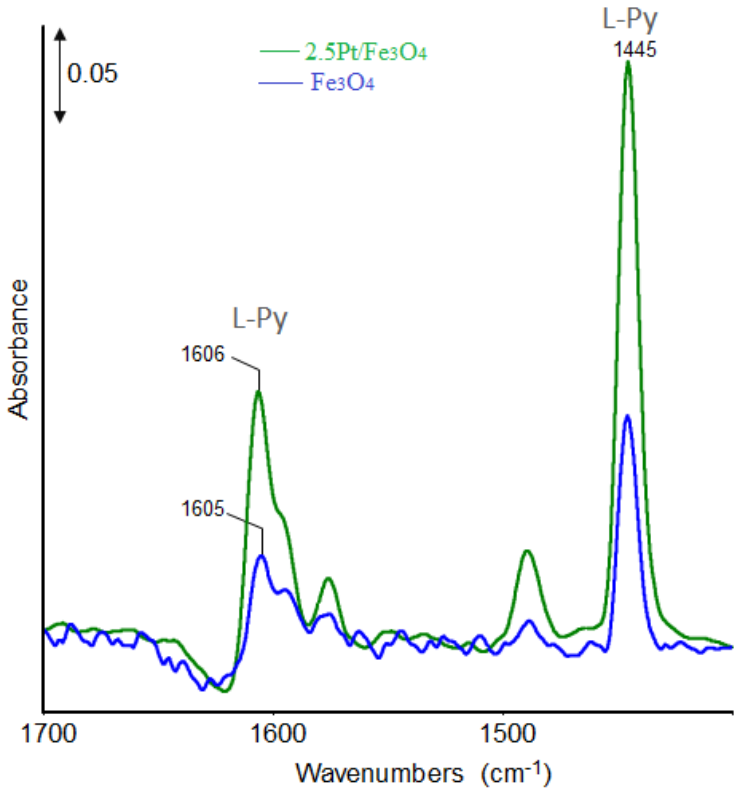

Figure 10: FT-IR spectra of pyridine adsorption on Fe_3O_4 and 2.5Pt/Fe_3O_4. The bands of Lewis acid sites are indicated as L-Py.

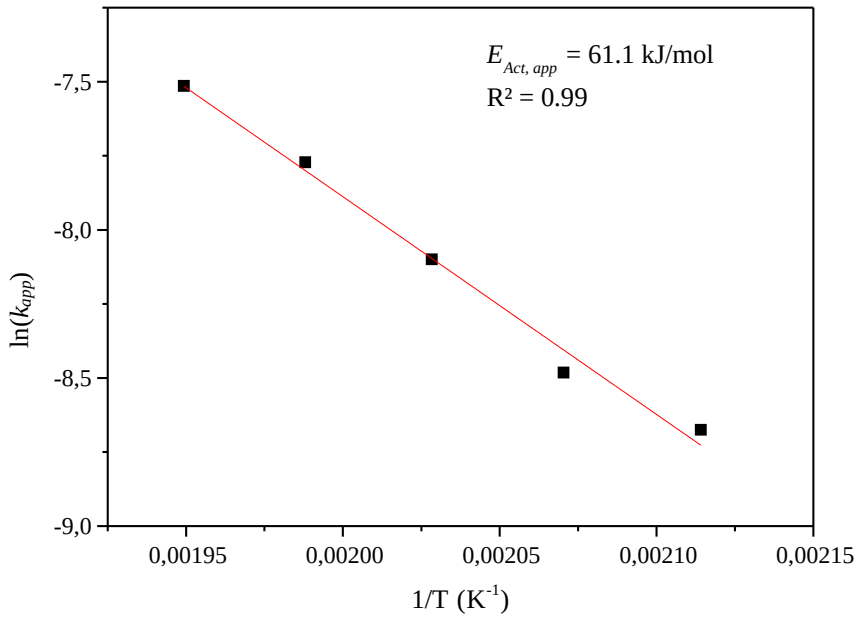

Figure 11: Arrhenius plot for apparent first order kinetic fit of APH of glycerol using 2.5Pt/Fe_3O_4.

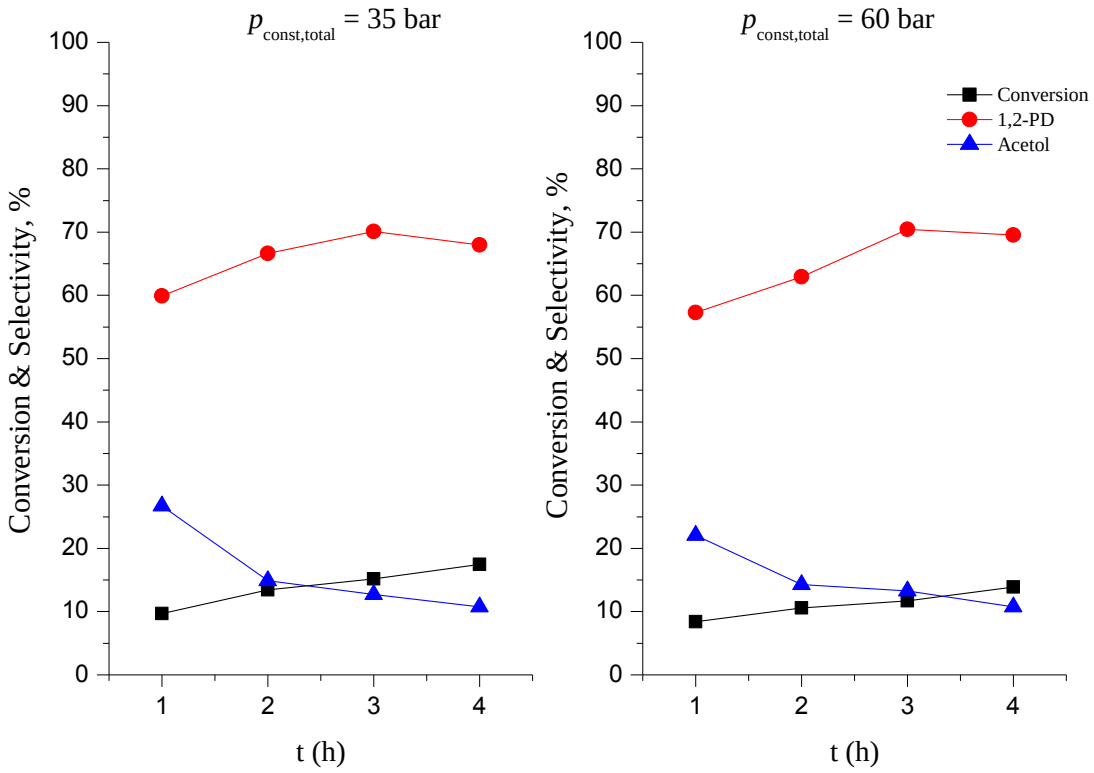

Figure 12: Kinetic effect of hydrogen partial pressure on glycerol conversion and selectivity for acetol and 1,2-PD in experiments at constant total pressure (i) 35 bar (p_{H2} = 10 bar), and (ii) 60 bar (p_{H2} = 35bar), both at 493 K.

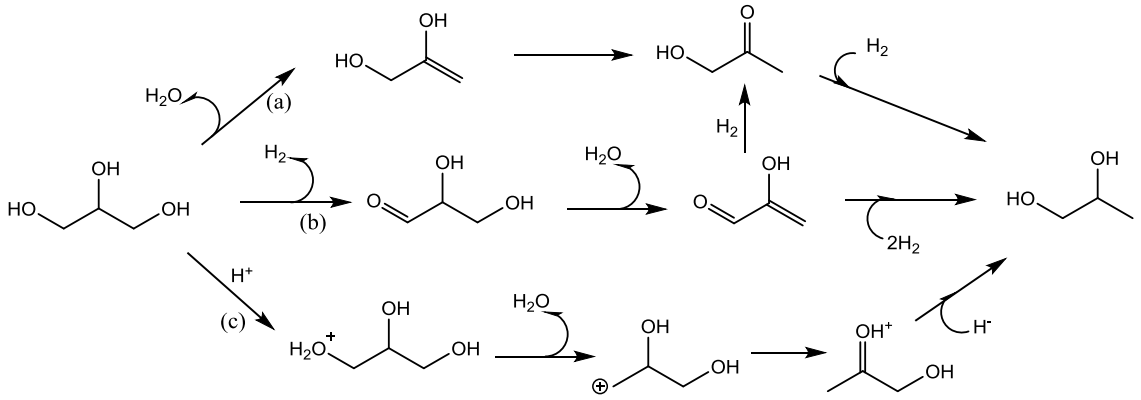

Figure 13: Scheme for 1,2-PD production via (a) the dehydration-hydrogenation route, (b) the dehydrogenation-dehydration-hydrogenation route and (c) the direct hydrogenation route.

Table 1. Elemental composition of Pt, Pd and Ni catalysts from ICP analysis.

Sample	Precursor /remarks	Fe content (wt%)		Pt, Pd, Ni content (wt%)	
		nominal	ICP	nominal	ICP
Fe_2O_3	-	69.9	67.6	-	-
2.5Pt/Fe_2O_3	$H_2PtCl_6 \cdot 6H_2O$	68.2	66.3	2.5	2.3
1.0Pt/Fe_2O_3	$H_2PtCl_6 \cdot 6H_2O$	69.2	67.9	1.0	0.97
2.5Pd/Fe_2O_3	$PdCl_2$	68.2	67.9	2.5	2.4
2.5Ni/Fe_2O_3	$NiCl_2$	68.2	68.3	2.5	2.5
2.5Pt/Fe_3O_4	Reduced catalyst (523 K)	70.5	67.8	2.5	2.4
2.5Pt/Fe_3O_4	Spent catalyst	70.5	67.5	2.5	2.6

Table 2. Surface texture and hydrogen chemisorption of support and Pt catalysts.

Material	BET surface area (m^2/g)	BJH pore diameter (nm)	Hydrogen chemisorption						
			1st uptake measure (µmol/g)	1st spillover degree (%)	2nd uptake measure (µmol/g)	2nd spillover degree (%)	3rd uptake measure (µmol/g)	Active particle diameter (nm)	Dispersion[a] (%)
Fe_2O_3	35.5	9.7	0.0		-		0.0	-	-
$1.0Pt/Fe_2O_3$	35.6	8.4	-		-		-	-	-
$2.5Pt/Fe_2O_3$	31.9	9.4	-		-		-	-	-
Fe_3O_4	-	-	0.0	-	-	-	-	-	-
$1.0Pt/Fe_3O_4$	30.8	12.1	111.4	434.9	83.8	327.2	18.2	1.6	71.0
$2.5Pt/Fe_3O_4$	24.7[b]	14.3[b]	201.4	314.3	212.3	331.4	40.7	1.8	63.6

[a]Considering the results of the 3rd uptake measure with unit H/Pt_{surf} stoichiometry.
[b]Spent catalyst after glycerol APH.

Table 3. Hydrogen uptake in TPR measurements for Ni, Pd and Pt catalysts supported on Fe_2O_3.

Material	Theoretical H_2 uptake (μmol/g)	H_2 uptake (μmol/g)	H_2 uptake from first peak (μmol/g)
Fe_2O_3	18785	19502	2335
2.5Pt/Fe_2O_3	19032	21680	3218
1.0Pt/Fe_2O_3	18712	18077	2727
2.5Pd/Fe_2O_3	19032	20477	2709
2.5Ni/Fe_2O_3	19032	21628	2395

Table 4. Amounts of desorbed CO_2 from TPD analysis.

Material	Impregnated metal (μmol/g)	Desorbed CO_2 (μmol/g)
Fe_2O_3	-	18.2
Fe_3O_4	-	29.1
2.5Pt/Fe_3O_4	128.1	31.5
2.5Pd/Fe_3O_4	235.0	34.6
2.5Ni/Fe_3O_4	425.9	38.0

Table 5. Activity and selectivity of selected Pt, Pd and Ni catalysts supported on iron oxide used in APH of glycerol.

Catalyst	Conversion[a]	Selectivity (%)					C Balance (%)[c]	
	(%)	1,2-PD	Acetol	1-PrOH	EG	Others[b]	GC	TOC
2.5Pt/Fe_3O_4	79.9	70.9	6.8	8.0	5.6	8.7	76.0	90.4
2.5Pt/Fe_3O_4[d]	69.5	68.0	7.7	10.1	5.4	8.7	80.7	96.4
1.0Pt/Fe_3O_4	46.5	76.1	10.1	4.2	5.4	4.3	99.5	97.2
1.0Pt/Fe_3O_4	81.0[e]	79.3	5.7	5.0	4.2	5.8	82.7	95.0
2.5Pd/Fe_3O_4	41.3	65.4	9.0	11.4	7.9	6.3	88.1	98.9
2.5Ni/Fe_2O_3	10.6	52.5	24.1	11.8	10.7	0.9	107.1	101.1
2.5Ni/Fe_3O_4[f]	5.7	28.2	37.0	12.9	20.3	1.6	101.4	98.1

[a]Conditions: *in situ* catalyst reduction; initial hydrogen pressure = 20 bar (gauge) at 433 K; 0.5 g_{cat}; 150 g of 10 wt% aqueous glycerol solution; 550 rpm; 16 hours, 503 K.

[b]In gas phase mainly CO_2 and CH_4; in liquid phase: ethanol, acetone, methanol.

[c]Carbon balance calculated from GC analyses of liquid phase products and from TOC analysis for liquid phase.

[d]Recycle run using the exact procedure and conditions with no previous treatment besides *in situ* pre-reduction.

[e]1.25 g_{cat}; 130 g of 10 wt% aqueous glycerol solution; 493 K.

[f]The catalyst sample was reduced at 673 K prior to introduction in the autoclave.

Table 6. Activity and selectivity of selected Pt, Pd and Ni catalysts supported on iron oxide applied to APR of glycerol.

Catalyst	T (K)	Conversion[a] (%)	Selectivity, H_2 yield (%)						C Balance[c] (%)
			1,2-PD	Acetol	1-PrOH	EG	Others[b]	H_2	
2.5Pt/Fe_3O_4	503	78.3	33.7	7.5	5.1	3.5	50.2	16.1	58.2
2.5Pt/Fe_3O_4	513	91.4	21.6	5.3	0.1	1.7	70.6	17.6	36.4
2.5Pd/Fe_3O_4	503	54.9	45.3	7.5	5.1	6.8	32.9	51.3	74.1
2.5Pd/Fe_3O_4	513	78.9	29.8	3.9	12.6	1.9	51.9	69.2	54.4
2.5Ni/Fe_3O_4[d]	503	5.8	15.2	36.5	16.7	17.4	14.2	1.2	100.7
2.5Ni/Fe_3O_4[d]	513	7.0	7.6	34.8	20.5	14.8	22.3	9.2	99.3
Fe_2O_3	503	4.8	19.4	40.8	17.9	21.5	0.3	7.7	103.7

[a]Conditions: *in situ* catalyst pre-reduction; argon initial pressure = 8 bar (gauge) at 298 K; 0.5 g_{cat}; 150 g of 10 wt% aqueous glycerol solution; 550 rpm; 16 hours.

[b]In gas phase mainly CO_2 and CH_4; in liquid phase: ethanol, acetone, methanol.

[c]Carbon balance from GC-FID analysis considering only liquid phase products.

[d]Reduced at 673 K prior to pre-reduction in the autoclave.

Table7. Conversion, selectivity and initial turnover frequency for APH of glycerol at different temperatures using $2.5Pt/Fe_3O_4$.

Temperature	Conversion[a]	Selectivity (%)					C Balance[c] (%)		TOF_0[d]
(K)	(%)	1,2-PD	Acetol	1-PrOH	EG	Others[b]	GC	TOC	(s^{-1})
463	17.6	64.6	9.7	3.8	9.5	12.4	104.6	103.7	-
473	22.6	67.9	8.7	4.0	9.8	9.6	91.8	99.3	0.014
483	51.8	79.1	7.4	3.1	7.1	3.3	91.9	94.4	0.046
493	67.1	78.8	6.8	4.5	5.8	4.1	95.2	99.3	0.065
503	79.9	70.9	6.8	8.0	5.6	8.7	76.0	90.4	0.094
513	86.2	58.2	9.0	15.9	5.7	11.1	65.7	86.6	0.121

[a]Conditions: *in situ* catalyst reduction; initial hydrogen pressure = 20 bar (gauge) at 433 K; 0.5 g_{cat}; 150 g of 10 wt% aqueous glycerol solution; 550 rpm; 16 hours.

[b]Other products are: ethanol, acetone, methanol, methane, CO_2.

[c]Carbon balance calculated from GC analyses of liquid phase products and by TOC analysis for liquid phase.

[d]Experiments done at 930 rpm, TOF calculated from initial reaction rate and taking H_2 chemisorption as a measure for amount of Pt_{surf}.

Table 8. APH of glycerol at different pressures using 2.5Pt/Fe_3O_4.

Pressure[a] (bar)	Conversion[b] (%)	Selectivity (%)				
		1,2-PD	Acetol	1-PrOH	EG	Others[c]
25	80.9	68.9	8.4	11.7	5.5	5.5
35	78.4	81.3	7.8	3.0	6.4	0.5
40	73.9	80.2	5.3	9.4	3.6	1.4
50	64.9	81.6	4.2	9.0	5.0	0.2

[a]Initial hydrogen pressures at 433 K.

[b]Conditions: reaction temperature: 503 K; *in situ* catalyst reduction; 0.5 g_{cat}; 150 mL of 10 wt% aqueous glycerol solution; 550 rpm; 16 hours.

[c]Other products are: ethanol, acetone, methanol, methane, CO_2.